Abdominal Imaging

Published online: 20 May 2011

Abdom Imaging (2012) 37:74–82
DOI: 10.1007/s00261-011-9758-1

Detection, classification, and characterization of focal liver lesions: Value of diffusion-weighted MR imaging, gadoxetic acid-enhanced MR imaging and the combination of both methods

Konstantin Holzapfel, Matthias J. Eiber, Alexander A. Fingerle, Melanie Bruegel, Ernst J. Rummeny, Jochen Gaa

Department of Radiology, Klinikum Rechts der Isar der Technischen Universität München, Ismaninger Str. 22, 81675 Munich, Germany

Abstract

Aim: To evaluate diffusion-weighted MR imaging (DWI), gadoxetic acid-enhanced MR imaging and the combination of both methods in the detection, classification, and characterization of focal liver lesions (FLL).
Methods: A total of 119 FLL (28 HCCs, 39 metastases, 15 FNHs, 11 adenomas, 13 hemangiomas, 13 cysts) were retrospectively analyzed in 36 patients. In those patients MR imaging of the liver comprising respiratory-triggered DWI (*b* values of 50, 300, and 600 s/mm^2) and gadoxetic acid-enhanced MR imaging including image acquisition in the hepatocyte-selective phase (20 min post injection) had been performed. Three image sets were assigned and compared: DWI only (set A), gadoxetic acid-enhanced MR imaging only (set B), and both modalities in combination (set C). Two readers independently interpreted the images in random order. For each reader and image set, the area under the receiver operating characteristic curve (Az) and sensitivity in the detection of FLL was determined as well as the accuracy in the classification and characterization of FLL.
Results: There was no significant difference between the three image sets in the detection of FLL with regards to Az. However, when only lesions with a diameter of 10 mm or less were analyzed, the Az values of set C were significantly higher than those of sets A and B for both readers. For classifying and characterizing FLL both set B and C were significantly superior to set A.
*Conclusion:*Adding DWI to gadoxetic acid-enhanced MR imaging significantly increases the accuracy in the detection of small FLL.

Correspondence to: Konstantin Holzapfel; *email:* holzapfel@roe.med.tum.de

Key words: Diffusion-weighted MR imaging (DWI)—Gadoxetic acid disodium—Magnetic resonance imaging—Focal liver lesions—Liver neoplasms

Introduction

Diffusion-weighted MR imaging (DWI) utilizes pulse sequences that are sensitive to diffusion (i.e., Brownian motion) of water protons and is increasingly being used in hepatic imaging due to recently improved imaging quality and compelling data suggesting a role of DWI in the detection and characterization of focal liver lesions (FLL) [1–9]. For example, recent studies have shown DWI to be superior to multi-slice computed tomography [10] and T2-weighted MR imaging in the detection of liver metastases [5] and to be a reasonable alternative to gadopentetate dimeglumine-enhanced MR imaging in the diagnosis of liver metastases [11].

MR imaging after the administration of liver-specific contrast agents is considered to be the best imaging modality in diagnosing FLL. However, a study conducted by Nasu et al. [12] showed a higher performance of DWI compared to SPIO-enhanced MR imaging in diagnosing liver metastases from colorectal cancer. In addition, adding DWI to a mangafodipir-enhanced MR imaging protocol increased the diagnostic accuracy in detecting colorectal liver metastases in a study conducted by Koh et al. [13]. Gadolinium-ethoxybenzyl-diethylenetriamine pentaacetic acid (gadoxetic acid disodium, Bayer Schering Pharma AG, Berlin, Germany) is a hepatocyte-specific MR imaging contrast agent. Owing to its hydrophilic, ionic, highly water-soluble nature it

can be administered by intravenous bolus injection. The potential to combine dynamic and hepatocyte-specific imaging within the same examination along with the high fraction of uptake by hepatocytes enabled improved detection and characterization of FLL using gadoxetic acid-enhanced MR imaging in several studies [e.g., 1, 14, 15]. Recently, Shimada et al. [16] compared gadoxetic acid-enhanced MR imaging and DWI in the detection of liver metastases. Performing a receiver operating characteristic (ROC) analysis, they found significant superiority of gadoxetic acid-enhanced MR imaging only in one of two independent, blinded readers, and no statistically significant difference between both modalities regarding sensitivity and positive predictive value (PPV) for both readers. A comparison of both modalities in combination to gadoxetic acid-enhanced MR imaging and DWI alone was not performed in that study. However, as some lesions detected by DWI were not seen by gadoxetic acid-enhanced MR imaging, the authors postulated that the combination of both methods may improve the detection of small hepatic metastases. To the best of the knowledge, an evaluation of both modalities (alone and in combination) in the classification (i.e., discrimination benign vs. malignant) and characterization of FLL has not been performed so far.

Therefore, the purpose of the study was to evaluate gadoxetic acid-enhanced MR imaging and DWI, alone and in combination, in the detection, classification, and characterization of FLL.

Materials and methods

Patients

The study was approved by the institutional review board. As images were analyzed retrospectively in this single-center study, the requirement for informed consent was waived. A query of the image database revealed a total of 91 patients with known or suspected FLL who had undergone gadoxetic acid-enhanced MR imaging and DWI of the liver at the institution between August 2006 and March 2010. Patients with hepatic neoplasms who had received local ablation therapy, chemotherapy, or radiation therapy within the last 3 months prior to the MR examination were excluded from the analysis in order to insure that the appearance of FLL on DWI was reflective of the natural state of the liver lesions ($n = 24$). In addition, patients without sufficient confirmation of the nature of the lesions were excluded (i.e., no histopathologic analysis, follow-up interval <6 months; $n = 25$). Finally, in six patients no FLL was confirmed by MR imaging and they were excluded from the study. Therefore, the final study population consisted of 36 patients (19 men, 17 women; mean age 55.5 ± 13.9 years, age range 32–77 years). There were 11 patients with history of an extrahepatic primary malignancy and known or suspected liver metastases (colorectal cancer [$n = 5$], breast cancer [$n = 3$], pancreatic cancer [$n = 1$], adenocarcinoma of the lung [$n = 1$], and liposarcoma [$n = 1$]). There were ten patients with chronic liver disease (including chronic hepatitis and cirrhosis related to hepatitis B/C or alcohol abuse). Finally, there were 15 patients with no history of malignancy or chronic liver disease who underwent MR imaging for evaluation of presumably benign or indeterminate, incidentally diagnosed FLL.

Standard of reference

Histopathologic confirmation of lesions was available in 17 patients (complete hepatectomy [$n = 1$], hemihepatectomy [$n = 1$], segmental or atypical liver resection [$n = 8$], and liver biopsy [$n = 7$]) within 30 days after MR imaging. In those patients, 13 hepatocellular carcinomas (HCCs), six metastases, five adenomas, and six focal nodular hyperplasias (FNHs) were confirmed.

In the remaining 19 patients, the standard of reference was represented by the consensus reading of two radiologists who were different from the blinded readers who performed the image analysis (see below). A malignant lesion (HCC or metastasis) was diagnosed, when there was new occurrence, growth (at least $>20\%$ relative or at least 5 mm absolute increase of the maximum initial diameter) or regression (complete disappearance or at least $>20\%$ relative or at least 5 mm absolute decrease of the maximum initial diameter) compared to prior MR imaging. In those cases, the diagnosis of a HCC was made when there was known chronic liver disease, an elevated serum concentration of alpha-1-fetoprotein (>10 ng/mL) and hyper enhancement compared to the surrounding liver parenchyma in the late arterial phase. In the remaining cases (all of those were patients with known extrahepatic primary malignancies) a metastasis was diagnosed. The remaining benign lesions were diagnosed by using established imaging criteria [17–19] in conjunction with stable appearance and size at follow-up imaging with a minimum follow-up interval of 6 months (mean follow-up period: 15.3 months, range: 6–36 months).

In the 36 patients included in this study, a total of 119 FLL was confirmed by the standard of reference: HCCs ($n = 28$), metastases ($n = 39$), solid benign FLL ($n = 26$; i.e., FNHs [$n = 15$] and hepatocellular adenomas [$n = 11$]), hemangiomas ($n = 13$), and cysts ($n = 13$). Mean diameter of FLL was 15.6 ± 7.2 mm (range: 4–42 mm). Forty-eight of the 119 FLL had a maximum diameter of 10 mm or less (9 HCCs, 24 metastases, 2 FNHs, 1 adenoma, 6 hemangiomas, 6 cysts).

MR imaging

MR imaging was performed on a 1.5-T system (Magnetom Avanto, Siemens Medical Solutions, Erlangen, Germany) with two six-channel body phased array coils

anterior and two spine clusters (three channels each) posterior. In addition to diffusion-weighted and gadoxetic acid-enhanced sequences (see below) at least a coronal T2-weighted half-Fourier single-shot turbo spin-echo (HASTE) sequence and an axial T2-weighted turbo spin-echo sequence were acquired.

Diffusion-weighted MR imaging (DWI). Diffusion-weighted images were acquired using a single-shot echo-planar imaging sequence. In order to acquire images with a high contrast-to-noise ratio for optimal conspicuity of FLL while keeping the influence of "pseudo-diffusion" by means of perfusion effects low, the minimum gradient factor (b value) was set at 50 s/mm^2. Thus, the gradient factors (b values) were 50, 300, and 600 s/mm^2. The technical parameters were as follows: echo time, 69 ms; echo train length, 58; echo spacing, 0.69 ms; receiver bandwidth, 1736 Hz/pixel; spectral fat saturation; field of view, 263 × 350 mm; matrix, 144 × 192; section thickness, 5 mm. For shortening of the echo train length, integrated parallel imaging techniques (iPAT) by means of generalized auto-calibrating partially parallel acquisitions (GRAPPA) with a twofold acceleration factor were used. For respiratory triggering, PACE (prospective acquisition correction) was implemented. Data was acquired during the end-expiratory phase. DWI was performed before the administration of gadoxetic acid.

Gadoxetic acid-enhanced MR imaging. Dynamic and delayed hepatocyte-selective phase T1-weighted, three-dimensional spoiled gradient-recalled echo images in the axial plane were obtained using a volumetric interpolated breath-hold examination (VIBE) sequence with spectral fat saturation (repetition time, 4.74 ms; echo time 2.38 ms; field of view, 380 × 309 mm; matrix, 320 × 182). Parallel imaging with a twofold acceleration factor (GRAPPA) was used. The initial VIBE sequence was acquired prior to the administration of the contrast agent. Subsequently, a bolus of 0.025 mmol/kg body weight gadoxetic acid (Bayer Schering Pharma AG, Berlin, Germany) was injected intravenously (antecubital vein) at a rate of 2.5 mL/s followed by 40 mL of a sterile isotonic saline solution. Three dynamic phases, late arterial (delay time 35 s), portal venous (70 s), and late dynamic (120 s) phases were acquired with a fixed delay. In addition, using the same VIBE sequence, images were acquired in the hepatocyte-selective phases 10 and 20 min after injection.

Image analysis

Review of all MR images and of all follow-up imaging (MRI, CT, PET-CT) was performed on a commercial PACS workstation (Easy vision, Philips, Best, The Netherlands). Three image datasets (DWI only: set A, gadoxetic acid-enhanced MR imaging only: set B, and both modalities in combination: set C) were evaluated by two independent readers with a time interval of at least 3 weeks between the analyses of the different datasets to avoid any recall bias. Images of the same dataset were analysed in random order. Readers were free to alter window level and window width at their discretion. Except for knowing that patients had been examined for known or suspected FLL, both readers were blinded to MR imaging reports, findings of other MR sequences, clinical history, and pathologic results.

Each reader documented the presence and segmental location—according to Couinaud's system of liver anatomy—of FLL using an ordinal five-point scale (1: definitely no FLL present, 2: probably no FLL present, 3: equivocal, 4: probably FLL present, 5: definitely FLL present). The sensitivity calculations were based only on those lesions awarded a confidence rating of 4 or 5. In case of multiple lesions per segment, the observers added information regarding size and location of the lesion within the segment to avoid confusion in the data analysis.

In addition, each seen FLL was classified as benign or malignant using an ordinal five-point scale (1: definitely benign, 2: probably benign, 3: indeterminate, 4: probably malignant, 5: definitely malignant). For lesions classified as malignant, readers were asked to characterize it as HCC or metastasis (see below). If a lesion was considered benign, readers were asked to characterize the lesion as a cyst, hemangioma, or solid benign lesion (FNH or adenoma) (see below).

In DWI (set A) primarily visual assessment of FLL was performed. A lesion was considered benign, when it was hyperintense at a low b value (b = 50 s/mm^2), showed a substantial (i.e., ≥50%) decrease in signal intensity at a high b value (b = 600 s/mm^2) and was hyperintense compared to the surrounding liver parenchyma on the ADC map. In equivocal cases, additionally, measurement of ADC values was performed. A circular region of interest (ROI) encompassing as much of a lesion as possible was drawn on the low b value (b = 50 s/mm^2) image (where all lesions show the highest conspicuity) and transferred to the ADC map. Corresponding to the experience from previous studies [8–10], a lesion was considered benign when an ADC value higher than 1.6 × 10^{-3} mm^2/s was measured. If a lesion was considered benign readers were asked to further classify the lesion as cyst, hemangioma, or solid benign lesion (FNH or adenoma) depending on the decrease in signal intensity between low (b = 50 s/mm^2) and high (b = 600 s/mm^2) b value images and the visually assessed ADC values with cysts showing the most pronounced signal loss and the highest ADC values followed by hemangiomas and solid benign lesions. Accordingly, a lesion was classified as malignant, when it was (moderately) hyperintense at b = 50 s/mm^2, remained hyperintense at b = 600 s/mm^2 and was iso- to

hypointense to adjacent liver parenchyma on the ADC map. Again, in equivocal cases the ADC value was measured, similarly as described for benign lesions. According to the experience from prior studies [8–10], a lesion was considered malignant when an ADC value lower than 1.4×10^{-3} mm^2/s was measured. If none of the criteria was met or ADC values between 1.4 and 1.6 ($\times 10^{-3}$ mm^2/s) were measured, a lesion was classified as indeterminate. In gadoxetic acid-enhanced MR imaging (set B) classification and characterization of FLL were performed using established imaging criteria both for dynamic and hepatocyte-selective imaging [14, 15, 17–26]. For the combined dataset (set C) readers were free to classify and characterize FLL according to the criterion providing the highest subjective confidence in each particular case.

Statistical analysis

Statistical analysis was performed using SPSS (version 16.0, SPSS Inc., Chicago, IL. USA) and Graph-Pad Prism 4 software package for Windows. For each image set, an ROC analysis was performed. The diagnostic accuracy for detecting FLL for each image set and for each reader was determined by measuring the area under the ROC curve (Az). The differences between the image sets (i.e., the mean Az values) were compared using the two-tailed Student's *t* test for paired samples. This analysis was performed for all lesions and, in a separate analysis, only for lesions with a maximum diameter of 10 mm or less. Likewise, sensitivities for the detection of FLL were calculated for each data set for each reader for all lesions and for lesions with a diameter of 10 mm or less. Sensitivities of the different datasets were compared using McNemar's test. In addition, the accuracies of each imaging set in classifying and characterizing FLL were calculated and compared using McNemar's test. Lesions that were not detected were considered as incorrectly classified/characterized. For each test a two-tailed *P* value of 0.05 was considered to indicate a statistically significant difference. Bonferroni correction was used for multiple pairwise comparisons.

Results

Results of analysis of each imaging set for each reader are summarized in Tables 1, 2, 3, 4, 5, and 6.

Detection of FLL

The calculated Az values for each image set are shown in Table 7. For both readers differences of Az values of the three image sets were not significantly different when all FLL were analyzed. However, performing an analysis of FLL with a diameter of 10 mm or less, Az values of set C were significantly higher than Az values of sets A and B for both readers. Sensitivities for detecting FLL were 90.76% (108/119 lesions, reader 1) and 88.24% (105/119 lesions, reader 2) for set A, 88.24% for both readers for set B (105/119 lesions), and 95.80% (114/119 lesions, reader 1) and 94.12% (112/119 lesions, reader 2) for set C. For both readers the difference of sensitivities between the three image sets A and B was not statistically significant ($P = 0.250$, $P = 0.420$). However, sensitivities of the combined dataset (set C) were significantly superior to sets A and B for both readers ($P = 0.031$ [A vs. C] and $P = 0.004$ [B vs. C] for reader 1; $P = 0.0156$ [A vs. C and B vs. C] for reader 2). When FLL with a diameter of 10 mm or less were analyzed separately, sensitivities of 79.17% (38/48, reader 1) and 75.00% (36/48, reader 2) for set A, 75.00% (36/48, reader 1) and 77.08% (37/48, reader 2) for set B and 91.67% (44/48, reader 1) and 89.58% (43/48, reader 2) for set C were obtained. Again, the sensitivity of set C in the detection of FLL was significantly superior to sets A and B ($P = 0.031$ [A vs. C] and $P = 0.008$ [B vs. C] for reader 1; $P = 0.016$ [A vs. C] and $P = 0.031$ [B vs. C] for reader 2), whereas there was no significant difference between sets A and B for both readers ($P = 0.480$, $P = 0.500$).

Table 1. Diagnosing FLL using DWI only—results for Reader 1

DWI only	Standard				
	Malignant lesions		Benign lesions		
	HCC	Metastasis	FNH/Adenoma	Hemangioma	Cyst
Malignant lesions					
HCC	12				
Metastasis	3	31	6	3	1
Benign lesions					
FNH/adenoma	2		17	1	
Hemangioma	4	5	1	9	
Cyst		1			12
Not seen	7	2	2		
	28	39	26	13	13

Table 2. Diagnosing FLL using gadoxetic acid-enhanced MR imaging only—results for Reader 1

Gadoxetic acid only	Standard				
	Malignant lesions		Benign lesions		
	HCC	Metastasis	FNH/Adenoma	Hemangioma	Cyst
Malignant lesions					
HCC	22				
Metastasis	1	29	2	1	1
Benign lesions					
FNH/adenoma	3		20	1	
Hemangioma		2	2	9	
Cyst		3			9
Not seen	2	5	2	2	3
	28	39	26	13	13

Table 3. Diagnosing FLL using both modalities—results for Reader 1

Both data sets	Standard				
	Malignant lesions		Benign lesions		
	HCC	Metastasis	FNH/Adenoma	Hemangioma	Cyst
Malignant lesions					
HCC	22				
Metastasis	1	35	2	1	1
Benign lesions					
FNH/adenoma	3		21	1	
Hemangioma		2	1	11	
Cyst		1			12
Not seen	2	1	2		
	28	39	26	13	13

Table 4. Diagnosing FLL using DWI only—results for Reader 2

DWI only	Standard				
	Malignant lesions		Benign lesions		
	HCC	Metastasis	FNH/Adenoma	Hemangioma	Cyst
Malignant lesions					
HCC	13				
Metastasis	1	29	7	2	2
Benign lesions					
FNH/adenoma	3		16		
Hemangioma	2	6	1	10	
Cyst		1		1	11
Not seen	9	3	2		
	28	39	26	13	13

As expected, most FLL not detected by DWI and gadoxetic acid-enhanced MR imaging were smaller than 10 mm, all of them had a diameter of less than 16 mm. Of the FLL missed by DWI and detected after administration of gadoxetic acid, five were located directly below the diaphragm or in the left liver lobe (Fig. 1). Seven lesions missed by gadoxetic acid-enhanced MR imaging but detected by DWI either showed subcapsular location in the right liver lobe or were located in immediate proximity of vessels (Fig. 2).

Classification of FLL

Using DWI only (set A), 72.27% (86/119) FLL were correctly classified as benign or malignant by reader 1 and 68.07% (81/119) by reader 2. Analyzing dataset B, readers 1 and 2 correctly classified 78.15% (93/119) and 77.31% (92/119) of lesions, respectively. Finally, using the combined dataset (set C) 91.23% (104/119) and 91.07% (102/119) of lesions were correctly classified by readers 1 and 2. For both readers, sets B and C were

Table 5. Diagnosing FLL using gadoxetic acid-enhanced MR imaging only—results for Reader 2

Gadoxetic acid only	Standard				
	Malignant lesions		Benign lesions		
	HCC	Metastasis	FNH/Adenoma	Hemangioma	Cyst
Malignant lesions					
HCC	22				
Metastasis	1	31	3	2	1
Benign lesions					
FNH/adenoma	2		19		
Hemangioma		3	2	8	1
Cyst		1			8
Not seen	3	4	2	3	3
	28	39	26	13	13

Table 6. Diagnosing FLL using both modalities—results for Reader 2

Both data sets	Standard				
	Malignant lesions		Benign lesions		
	HCC	Metastasis	FNH/Adenoma	Hemangioma	Cyst
Malignant lesions					
HCC	22				
Metastasis	1	34	3	1	1
Benign lesions					
FNH/adenoma	2		20		
Hemangioma		2	1	12	
Cyst		1			12
Not seen	3	2	2		
	28	39	26	13	13

Table 7. Area under the receiver operating characteristic curve (Az) for each dataset and reader

All lesions (n = 119)	Reader 1	Reader 2
Set A	0.933 ± 0.019	0.928 ± 0.019
Set B	0.937 ± 0.018	0.911 ± 0,022
Set C	0.957 ± 0.014	0.929 ± 0.021
Lesions ≤10 mm (n = 48)	**Reader 1**	**Reader 2**
Set A	0.807 ± 0.044	0.772 ± 0.049
Set B	0.805 ± 0.043	0.812 ± 0.049
Set C	0.870 ± 0.040	0.894 ± 0.039

The differences between Az values of the three data sets for all lesions are not significantly different for both readers.
Az values are presented as mean ± standard deviation
For lesions ≤10 mm Az values of set C are significantly higher than those of sets A and B for both readers (P = 0.001 [A vs. C] and P = 0.002 [B vs. C] for reader 1; P = 0.046 [A vs. C] and P = 0.005 [B vs. C] for reader 2)

significantly superior to set A (P = 0.016 [A vs. B] and $P < 0.0001$ [A vs. C] for reader 1; P = 0.001 [A vs. B] and $P < 0.0001$ [A vs. C] for reader 2) and set C was significantly superior to set B (P = 0.001 for reader 1; P = 0.002 for reader 2).

Characterization of FLL

Reader 1 correctly characterized 68.07% (81/119) and reader 2 66.39% (79/119) of lesions using set A. For set B the values were 74.79% (89/119, reader 1) and 73.95% (88/119, reader 2), respectively. Finally, analyzing both modalities in combination (set C), 84.87% (101/119) of lesions were correctly characterized by reader 1 and 84.03% (100/119) by reader 2. Again, sets B and C were significantly superior to set A (P = 0.016 [A vs. B] and $P < 0.0001$ [A vs. C] for reader 1; P = 0.004 [A vs. B] and $P < 0.0001$ [A vs. C] for reader 2), and set C was significantly superior to set B (P = 0.0005 for readers 1 and 2).

Discussion

Correct detection, classification, and characterization of FLL are of paramount importance as they may significantly affect the choice of therapeutic approach in many cases. In this study, there was no significant difference between DWI and gadoxetic acid-enhanced MR imaging regarding accuracy and sensitivity in the detection of FLL. The high lesion-to-liver contrast and the ''black blood'' effect allowed detecting even small FLL with a diameter of 10 mm or less. Especially, some lesions in close proximity of vessels and subcapsular lesions in the

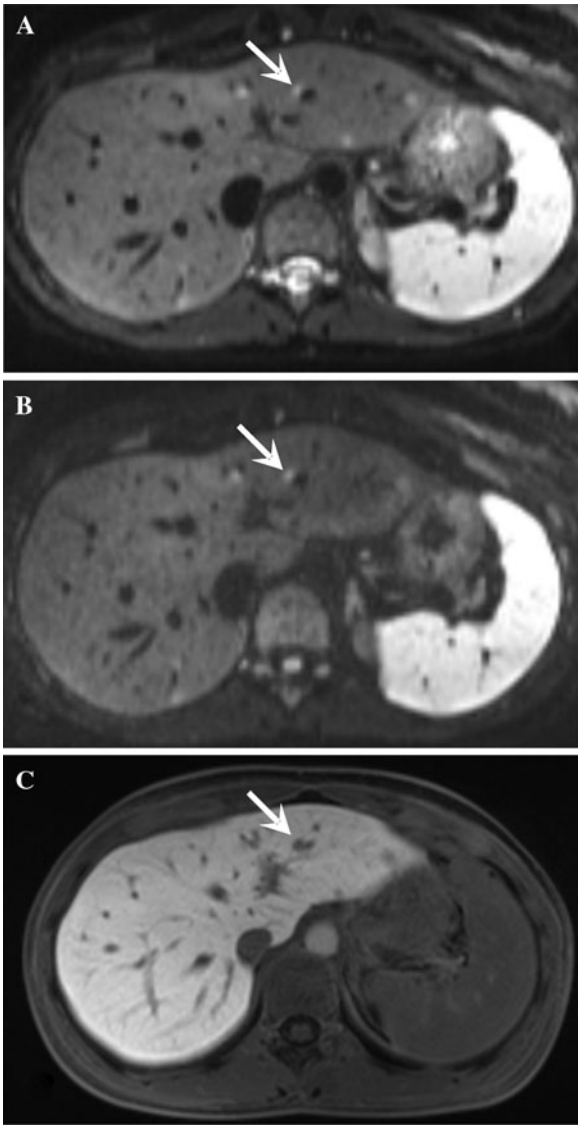

Fig. 1. MR images of a 39-year-old woman with breast cancer. Among other small metastases, there is a small lesion in the left liver lobe (*arrow*) that is clearly hyperintense both at $b = 50$ s/mm^2 (**A**) and $b = 600$ s/mm^2 (**B**) and, therefore, suspicious for a metastasis. As the lesion is located in immediate proximity to a vessel, although retrospectively visible, it was not detected by gadoxetic acid-enhanced MR imaging (**C**) by both readers (20 min post injection)

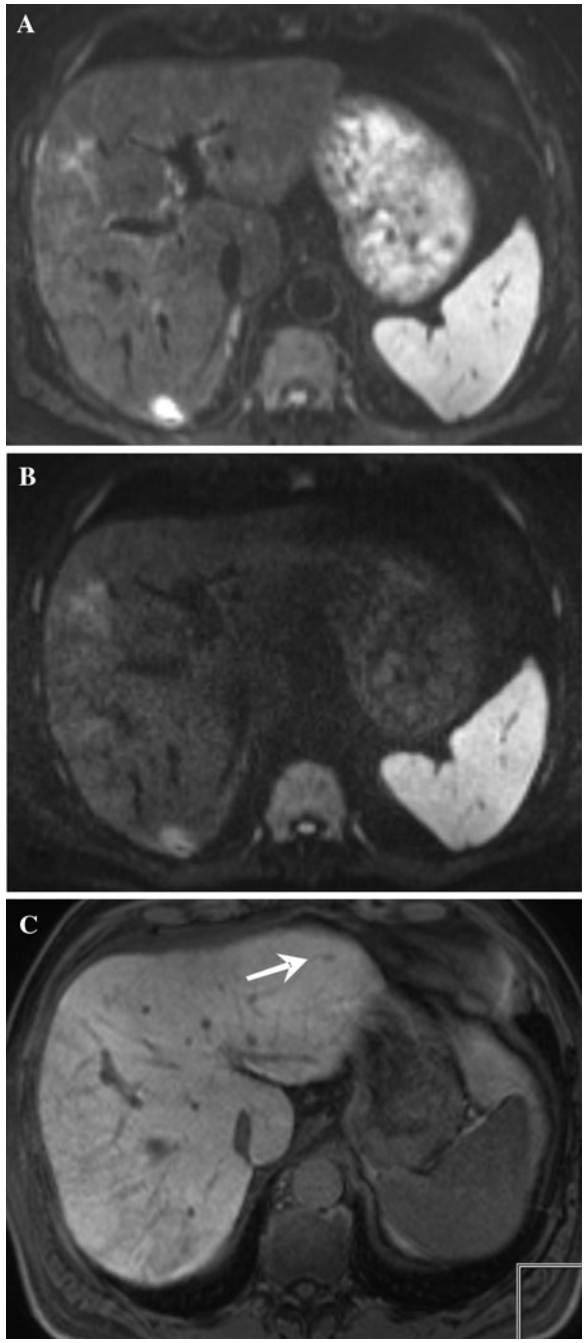

Fig. 2. MR images of a 62-year-old man with colorectal cancer. In the left liver lobe no focal liver lesion is seen at $b = 50$ s/mm^2 (**A**) and $b = 600$ s/mm^2 (**B**) in DWI. However, although subtle, gadoxetic acid-enhanced MR imaging (**C**) (20 min post injection) reveals a small hypointense lesion (*arrow*). In follow-up imaging considerable growth confirmed a metastasis

right liver lobe could be detected by DWI only. However, as described before, due to artefacts (i.e., motion and pulsation from stomach and heart, air within the stomach), DWI has some limitations in the detection of FLL localized adjacent to the stomach in the left liver lobe and of lesions immediately below the diaphragm. Az values and sensitivities in this study are in the same range as reported by Shimada et al. [16], who evaluated both modalities in the detection of small hepatic metastases. In contrast to this study Shimada et al. found significantly higher Az values for one of two independent observers at a 3-T MR system, however, without any significant differences regarding sensitivities. One potential explanation for this difference, although speculative, may be the different field strengths used in both

studies, as achieving the same image quality without image distortions by artefacts to the experience seems to be more challenging at 3T.

In this study for the first time the value of DWI and gadoxetic acid-enhanced MR imaging in combination was compared to both modalities alone. For both readers, the combined image set showed significantly higher sensitivities in the detection of FLL and higher Az values when only lesions with a diameter of 10 mm or less were analyzed. This demonstrates that, as mentioned above, both modalities have strengths and weaknesses and complement one another especially in the detection of small FLL. As hepatocyte-selective imaging requires a delay of 20 min and as recent studies have shown that both modalities do not negatively influence each other [27, 28], DWI may be added to the imaging protocol in the time period between dynamic imaging and the hepatocyte-selective phase without any additional expenditure of time.

DWI has been shown to be a potential supplementary tool in the classification and characterization of FLL both by visual evaluation and by ADC measurement [7–9]. However, in those studies limitations in this task have been described, i.e., for example strong overlap of ADC values of malignant FLL with solid benign liver lesions (FNH, adenoma) which therefore cannot be reliably differentiated by DWI only. Consequently, in this study, DWI performed significantly inferior to gadoxetic acid-enhanced imaging in classifying and characterizing FLL. However, it has to be mentioned that the population in this study is a pre-selected cohort of patients with many patients undergoing MR imaging of the liver because of equivocal imaging findings in other modalities and a comparably high fraction of solid benign FLL. Therefore, the difference between DWI and gadoxetic acid-enhanced MR imaging may be less evident in a less pre-selected patient population. Surprisingly, for both readers the combination of both modalities was significantly superior to gadoxetic acid-enhanced MR imaging alone in classifying and characterizing FLL. This may be explained by the higher fraction of hemangiomas and cysts that were correctly diagnosed by DWI as readers were not allowed to view T2-weighted images. Hence, this finding probably presents an artificial result and is a potential limitation of this study. In addition, some very small cysts and hemangiomas were not detected using gadoxetic acid-enhanced MR imaging and, thus, could not be classified and characterized correctly.

The study has several limitations. First, this is a retrospective analysis of patients undergoing MR imaging of the liver including DWI, gadoxetic acid-enhanced MR imaging and follow-up imaging. Thus, there is the possibility of selection bias and, consequently, overestimation of the accuracies of both modalities in the diagnosis of FLL. Second, histopathologic confirmation was available only in 17 out of 36 patients. Obtaining histopathologic diagnosis in all patients would be desirable, but this is not clinically and ethically appropriate in most cases. However, a thorough review of all MR sequences and of follow-up imaging was performed by two readers, leading to a low probability of misclassification of lesions. Third, the slice thickness of the contrast-enhanced VIBE sequence was 3 mm compared to 5 mm for DWI. However, the use of modern high resolution, three-dimensional gradient-recalled echo sequences is well-established in clinical routine, and the use of a two-dimensional sequence with a higher slice thickness only for comparison would probably lead to a deterioration of diagnostic performance, especially for small FLL, and may not be feasible, neither clinically nor ethically.

In conclusion, in this study, combining DWI and gadoxetic acid-enhanced MR imaging helped to significantly improve the accuracy and the sensitivity in the detection of FLL, in particular of lesions with a diameter of 10 mm or less. Therefore, as the quality of diffusion-weighted images is not reduced when DWI is performed after application of the contrast agent, DWI could be added to the liver imaging protocol between the dynamic and the hepatocyte-selective phase without any additional expenditure of time. In addition, although significantly inferior to gadoxetic acid-enhanced MR imaging, DWI may be used as a supplementary method in the classification and characterization of FLL in particular cases, e.g., to diagnose very small cysts or hemangiomas that are not visible in other MR sequences.

References

1. Namimoto T, Yamashita Y, Sumi S, Tang Y, Takahashi M (1997) Focal liver masses: characterization with diffusion-weighted echo-planar MR imaging. Radiology 204:739–744
2. Taouli B, Vilgrain V, Dumont E, et al. (2003) Evaluation of liver diffusion isotropy and characterization of focal hepatic lesions with two single-shot echo-planar MR imaging sequences: prospective study in 66 patients. Radiology 226:71–78
3. Coenegrachts K, Delanote J, Ter Beek L, et al. (2007) Improved focal liver lesion detection: comparison of single-shot diffusion-weighted echoplanar and single-shot T2 weighted turbo spin echo techniques. Br J Radiol 80:524–531
4. Parikh T, Drew SJ, Lee VS, et al. (2008) Focal liver lesion detection and characterization with diffusion-weighted MR imaging: comparison with standard breath-hold T2-weighted imaging. Radiology 246:812–822
5. Bruegel M, Gaa J, Waldt S, et al. (2008) Diagnosis of hepatic metastasis: comparison of respiration-triggered diffusion-weighted echo-planar MRI and five t2-weighted turbo spin-echo sequences. AJR Am J Roentgenol 191:1421–1429
6. Zech CJ, Herrmann KA, Dietrich O, et al. (2008) Black-blood diffusion-weighted EPI acquisition of the liver with parallel imaging: comparison with a standard T2-weighted sequence for detection of focal liver lesions. Invest Radiol 43:261–266
7. Gourtsoyianni S, Papanikolaou N, Yarmenitis S, et al. (2008) Respiratory gated diffusion-weighted imaging of the liver: value of apparent diffusion coefficient measurements in the differentiation between most commonly encountered benign and malignant focal liver lesions. Eur Radiol 18:486–492
8. Bruegel M, Holzapfel K, Gaa J, et al. (2008) Characterization of focal liver lesions by ADC measurements using a respiratory triggered diffusion-weighted single-shot echo-planar MR imaging technique. Eur Radiol 18:477–485

9. Holzapfel K, Bruegel M, Eiber M, et al. (2010) Characterization of small (≤10 mm) focal liver lesions: value of respiratory-triggered echo-planar diffusion-weighted MR imaging. Eur J Radiol 76: 89–95
10. Holzapfel K, Reiser-Erkan C, Fingerle AA,et al. (2010) Comparison of diffusion-weighted MR imaging and multidetector-row CT in the detection of liver metastases in patients operated for pancreatic cancer. Abdom Imaging. doi: 10.1007/s00261-010-9633-5
11. Hardie AD, Naik M, Hecht EM, et al. (2010) Diagnosis of liver metastases: value of diffusion-weighted MRI compared with gadolinium-enhanced MRI. Eur Radiol 20:1431–1441
12. Nasu K, Kuroki Y, Nawano S, et al. (2006) Hepatic metastases: diffusion-weighted sensitivity-encoding versus SPIO-enhanced MR imaging. Radiology 239:122–130
13. Koh DM, Brown G, Riddell AM, et al. (2008) Detection of colorectal hepatic metastases using MnDPDP MR imaging and diffusion-weighted imaging (DWI) alone and in combination. Eur Radiol 18:903–910
14. Zech CJ, Herrmann KA, Reiser MF, Schoenberg SO (2007) MR imaging in patients with suspected liver metastases: value of liver-specific contrast agent Gd-EOB-DTPA. Magn Reson Med Sci 6:43–52
15. Huppertz A, Balzer T, Blakeborough A, et al. (2004) Improved detection of focal liver lesions at MR imaging: multicenter comparison of gadoxetic acid-enhanced MR images with intraoperative findings. Radiology 230:266–275
16. Shimada K, Isoda H, Hirokawa Y, et al. (2010) Comparison of gadolinium-EOB-DTPA-enhanced and diffusion-weighted liver MRI for detection of small hepatic metastases. Eur Radiol 20:2690–2698
17. Semelka RC, Brown ED, Ascher SM, et al. (1994) Hepatic hemangiomas: a multi-institutional study of appearance on T2-weighted and serial gadolinium-enhanced gradient-echo MR images. Radiology 192:401–406
18. Bartolozzi C, Cioni D, Donati F, Lencioni R (2001) Focal liver lesions: MR imaging pathologic correlation. Eur Radiol 11: 1374–1388
19. Horton KM, Bluemke DA, Hruban RH, Soyer P, Fishman EK (1999) CT and MR imaging of benign hepatic and biliary tumors. Radiographics 19:431–451
20. Vogl TJ, Kümmel S, Hammerstingl R, et al. (1996) Liver tumors: comparison of MR imaging with Gd-EOB-DTPA and Gd-DTPA. Radiology 200:59–67
21. Hammerstingl R, Huppertz A, Breuer J, et al. (2008) Diagnostic efficacy of gadoxetic acid (Primovist)-enhanced MRI and spiral CT for a therapeutic strategy: comparison with intraoperative and histopathologic findings in focal liver lesions. Eur Radiol 18:457–467
22. Huppertz A, Haraida S, Kraus A, et al. (2005) Enhancement of focal liver lesions at gadoxetic acid-enhanced MR imaging: correlation with histopathologic findings and spiral CT–initial observations. Radiology 234:468–478
23. Saito K, Kotake F, Ito N, et al. (2005) Gd-EOB-DTPA enhanced MRI for hepatocellular carcinoma: quantitative evaluation of tumor enhancement in hepatobiliary phase. Magn Reson Med Sci 4:1–9
24. Sun HY, Lee JM, Shin CI, Lee DH, et al. (2010) Gadoxetic acid-enhanced magnetic resonance imaging for differentiating small hepatocellular carcinomas (< or = 2 cm in diameter) from arterial enhancing pseudolesions: special emphasis on hepatobiliary phase imaging. Invest Radiol 45:96–103
25. Brody JM, Schafer L, Tung GA, Breuer J, Shamsi K (2005) Conspicuity of liver hemangiomas: short tau inversion recovery, T1, and T2 imaging with gadolinium ethoxybenzyl diethylenetriaminepentaacetic acid. J Magn Reson Imaging 21:391–397
26. Zech CJ, Grazioli L, Breuer J, Reiser MF, Schoenberg SO (2008) Diagnostic performance and description of morphological features of focal nodular hyperplasia in Gd-EOB-DTPA-enhanced liver magnetic resonance imaging: results of a multicenter trial. Invest Radiol 43:504–511
27. Choi JS, Kim MJ, Choi JY, et al. (2010) Diffusion-weighted MR imaging of liver on 3.0-Tesla system: effect of intravenous administration of gadoxetic acid disodium. Eur Radiol 20:1052–1060
28. Choi SA, Lee SS, Jung IH, et al. (2010) The effect of gadoxetic acid enhancement on lesion detection and characterisation using T2 weighted imaging and diffusion weighted imaging of the liver. Br J Radiol. doi:10.1259/bjr/12929687